Int. J. Multiphase Flow, Vol. 2, pp. 191–212. Pergamon/Elsevier, 1975. Printed in Great Britain

THE APPLICABILITY OF DYNAMIC-SIMILARITY CRITERIA TO ISOTHERMAL, LIQUID–GAS, TWO-PHASE FLOWS WITHOUT MASS TRANSFER

A. K. CHESTERS

Laboratory for Aero- and Hydrodynamics, Delft University of Technology, The Netherlands

(*Received* 1 *June* 1974)

Abstract—It is demonstrated that simple similarity criteria which can be satisfied experimentally can be derived from the conventional equations governing gas–liquid flows. The criteria are thus susceptible to experimental verification and potentially useable for the scaling of flows. The convention equations, however, are seen to break down in the context of rupturing films or filaments, in particular owing to the special influences of van der Waals forces. The validity of the criteria in any given case rests on the influence of such special effects on the general flow development. Two cases are examined, coalescing bubbles and atomising liquid sheets, and the influence of van der Waals forces on the rupture time shown to be slight.

1. INTRODUCTION

In the field of single-phase flow, the use of dynamic-similarity criteria is standard procedure, the principal advantages being:

(1) The possibility of testing a system under "scaled" but equivalent conditions;

(2) a much more concise description of flow phenomena as functions of the similarity parameters than of individual fluid properties;

(3) the use of the simplest criteria for isothermal or adiabatic flows as a starting point for more general criteria for flows with heat and mass transfer.

In the field of two-phase flow the number or variables is much greater and the need to regroup these into the smallest number of influencing parameters would seem especially great. Surprising, however, little mention and hardly any use has been made of the similarity approach although a number of inexact empirical correlations for two-phase flow behaviour are in use.

In the present paper the following steps are taken.

(1) The conventional physical model of isothermal liquid–gas flows is used to derive the simplest possible general criteria for dynamic similarity.

(2) The possibility of experimentally satisfying these criteria is considered. This is seen to be feasible under certain circumstances, so that an experimental test of the criteria's validity is possible, as well as limited practical scaling of flows given such validity.

(3) The assumptions of the conventional physical model of isothermal flows are examined closely and seen to be suspect for flows with joining or dividing phase boundaries, because of special effects present in very thin films and filaments.

(4) Two such flows (coalescing bubbles and atomising liquid sheets) are examined in more detail to ascertain whether the conventional model is likely to suffice.

In (4) some of the ideas introduced about the mechanisms of coalescence and sheet break up are new.

2. THE CONVENTIONAL PHYSICAL MODEL AND THE RELATED SIMILARITY CRITERIA

The conventional model of isothermal gas–liquid flows is that of two Newtonian fluids, each satisfying its own equation of state, continuity and Navier–Stokes, the conventional no-slip condition at solid boundaries and the following conditions at liquid–gas interfaces:

1. Continuity of velocity (i.e. a further no-slip condition);
2. continuity of tangential stress;
3. a discontinuity in normal stress given by

$$P'_G - P'_L = \sigma\left(\frac{1}{R_1'} + \frac{1}{R_2'}\right).$$

Here P'_G and P'_L are the normal stresses in the gas and liquid respectively, R'_1 and R'_2 the radii of curvature of the interface in any two planes containing the normal, and σ, the surface tension, is a constant.

By dynamic similarity of two such flows is meant that their velocity fields are identical at all times when expressed in terms of distances, velocities and times normalized with respect to a characteristic length and velocity of the flow. Written in such normalized terms (making use, additionally, of the liquid density as characteristic density) the governing equations are as follows.

The gas

Navier–Stokes:

$$\frac{\mathrm{D}\mathbf{u}_G}{\mathrm{D}t} = \left(\frac{1}{F}\right)\mathbf{k} - \left(\frac{1}{\rho_G}\right)\operatorname{grad} p_G + \left(\frac{\mu_G}{\rho_G}\right)\left(\frac{1}{3}\operatorname{grad}\operatorname{div}\mathbf{u}_G + \operatorname{grad}^2\mathbf{u}_G\right) \quad [1]$$

Continuity:

$$\frac{\mathrm{D}\rho_G}{\mathrm{D}t} = -\rho_G \operatorname{div}\mathbf{u}_G \quad [2]$$

State:

$$\frac{p_G}{\rho_G} = \text{constant} = E. \quad [3]$$

The liquid

Navier–Stokes:

$$\frac{\mathrm{D}\mathbf{u}_L}{\mathrm{D}t} = \left(\frac{1}{F}\right)\mathbf{k} - \operatorname{grad} p_L + \left(\frac{1}{Re_L}\right)\operatorname{grad}^2\mathbf{u}_L \quad [4]$$

Continuity:

$$\operatorname{div}\mathbf{u}_L = 0 \quad [5]$$

State (already incorporated in [4] and [5]):

$$\rho_L = 1. \quad [6]$$

The interface

Continuity of velocity:

$$\mathbf{u}_G = \mathbf{u}_L \quad [7]$$

Continuity of tangential stress:

$$\mu_G\left(\frac{\partial w_G}{\partial x} + \frac{\partial u_G}{\partial z}\right) = \left(\frac{1}{Re_L}\right)\left(\frac{\partial w_L}{\partial x} + \frac{\partial u_L}{\partial z}\right) \quad [8]$$

$$\mu_G\left(\frac{\partial w_G}{\partial y} + \frac{\partial v_G}{\partial z}\right) = \left(\frac{1}{Re_L}\right)\left(\frac{\partial w_L}{\partial y} + \frac{\partial v_L}{\partial z}\right) \quad [9]$$

Discontinuity in normal stress:

$$\left[-p_G + 2\mu_G\left(\frac{\partial w_G}{\partial z} - \frac{1}{3}\operatorname{div}\mathbf{u}_G\right)\right] - \left[-p_L + \left(\frac{2}{Re_L}\right)\frac{\partial w_L}{\partial z}\right] = \left(\frac{1}{W}\right)\left(\frac{1}{R_1} + \frac{1}{R_2}\right). \quad [10]$$

Here $\mathbf{u}$, ρ, p, μ and t denote the normalized velocity, density, pressure, dynamic viscosity and time respectively, div, grad and grad^2 are with respect to normalized distance, and the subscripts G and L denote gas and liquid. x, y and z are normalized Cartesian coordinates defined at the point of the interface under consideration, z having the direction of the local interface normal. u, v and w are the associated normalized velocity components. Thus, although the laws expressed by [8], [9] and [10] apply over the whole interface, the direction of z varies from point to point, adjacent directions being related by the interface curvature. $\mathbf{k}$ is the unit vector in the vertical downwards direction.

It is seen that provided the five dimensionless constants F (Froude number, u_C^2/gx_C), Re_L (liquid Reynolds number, $u_C x_C \rho'_L/\mu'_L$), W (Weber number, $u_C^2 x_C \rho'_L/\sigma$), E (Euler number, $p'_G/\rho'_G u_C^2$) and $\mu_G(\mu'_G/u_C x_C \rho'_L)$ are equal for two flows the normalized governing equations are identical. Here primed symbols denote the original, dimensional variables, g is the (dimensional) acceleration due to gravity, and u_C and x_C are a characteristic (dimensional) velocity and length. Provided also that the normalized boundary conditions are the same for each flow, dynamic similarity will result. In addition to geometrically similar distributions of imposed pressure or velocity, the latter implies equal ρ_G at some characteristic point in the flow at all normalized times:

$$\rho_{G,C} = \rho'_{G,C}/\rho'_L = \text{identical} \qquad [11]$$

where C again stands for characteristic and "identical" is used to mean equal in both flows. The requirement of equal Euler number is satisfied everywhere if satisfied at some characteristic point at all normalized times:

$$E = p'_{G,C}/\rho'_{G,C} u_C^2 = \text{identical.}$$

Equivalently, from [11],

$$p'_{G,C}/\rho'_L u_C^2 = \text{identical.} \qquad [12]$$

Listing the remaining requirements

$$F = u_C^2/gx_C = \text{identical} \qquad [13]$$

$$Re_L = u_C x_C \rho'_L/\mu'_L = \text{identical} \qquad [14]$$

$$W = u_C^2 x_C \rho'_L/\sigma = \text{identical} \qquad [15]$$

$$\mu_G = \mu'_G/u_C x_C \rho'_L = \text{identical.}$$

In view of [14] the latter can be given more simply as

$$\mu'_G/\mu'_L = \text{identical.} \qquad [16]$$

3. EXPERIMENTAL SATISFACTION OF THE CRITERIA

Given the validity of the conventional physical model six conditions, [11]–[16], must therefore be satisfied, in addition to geometrical similarity of imposed boundary conditions in order to obtain dynamic similarity of two isothermal liquid–gas flows. This situation may be compared with that of single-phase isothermal flow where only one condition, equal Re_L, need be satisfied in the case of liquids or two, equal Re_G and E (= [isothermal Mach number]$^{-2}$), in the case of gases. Surprisingly, however, it appears possible to satisfy all six requirements under certain conditions.

Consider first the three requirements [13], [14] and [15]. With a little algebraic manipulation

these can be re-expressed as:

$$u_C = \left(\frac{FWg\sigma}{\rho_L'}\right)^{1/4},$$

i.e.

$$\frac{(u_C)_1}{(u_C)_2} = \frac{(\sigma/\rho_L')_1^{1/4}}{(\sigma/\rho_L')_2^{1/4}}, \qquad [17]$$

assuming g to be equal for the two flows, 1 and 2,

$$x_C = \left(\frac{W\sigma}{F\rho_L' g}\right)^{1/2},$$

i.e.

$$\frac{(x_C)_1}{(x_C)_2} = \frac{(\sigma/\rho_L')_1^{1/2}}{(\sigma/\rho_L')_2^{1/2}}, \qquad [18]$$

and

$$\frac{\sigma^3\rho_L'}{g(\mu_L')^4} = \frac{(Re_L)^4 F}{W^3} = Q = \text{identical}. \qquad [19]$$

[17] and [18] stipulate the relative sizes and velocities of the two flows, which are completely determined once the liquids are chosen. [19] restricts the choice of liquids to those having the same value of the property parameter Q. Some examples of Q values at 20°C are given below.

Liquid	ρ_L'(kgm^{-3})	σ(kgsec^{-2})	μ_L'(kgm^{-1}s^{-1})	Q
Mercury	13.6×10^3	472×10^{-3}	1.56×10^{-3}	2.46×10^{13}
Water	1.00×10^3	72.8×10^{-3}	1.00×10^{-3}	3.93×10^{10}
Trichloroethylene	1.46×10^3	29.3×10^{-3}	0.56×10^{-3}	3.81×10^{10}
Ethanol	0.79×10^3	22.8×10^{-3}	1.20×10^{-3}	4.60×10^{8}

While most of the liquids are clearly "unscalable" by each other, the Q values for water and trichloroethylene are very close. Since Q is a steep function of temperature, only a small change in the temperature of either liquid is necessary to equalize the values. The required length and velocity scale factors are given by [17] and [18]:

$$\frac{(u_C)_{tr}}{(u_C)_w} \simeq 0.72; \quad \frac{(x_C)_{tr}}{(x_C)_w} \simeq 0.53.$$

The satisfaction of [12] is, in principle, always possible by appropriate adjustment of the absolute pressure:

$$\frac{(p_{G,C}')_1}{(p_{G,C}')_2} = \frac{(\rho_L' u_C^2)_1}{(\rho_L' u_C^2)_2} = \frac{(\sigma\rho_L')_1^{1/2}}{(\sigma\rho_L')_2^{1/2}} \qquad [20]$$

from [17]. For the case of trichloroethylene and water $(p_{G,C}')_{tr}/(p_{G,C}')_w \simeq 0{\cdot}77$.

The satisfaction of [11] will be possible in many instances because of the miscibility of all gases and the wide range of gas densities. From [11], [20] and the perfect gas law the required ratio of molecular weights is

$$\frac{(MW)_1}{(MW)_2} = \frac{(\rho_L'/\sigma)_1^{1/2}}{(\rho_L'/\sigma)_2^{1/2}} \cdot \frac{T_1}{T_2}, \qquad [21]$$

where T denotes absolute temperature.

The final requirement, satisfaction of [16], will be possible in fewer cases because of the small range of μ_G'. For the case of trichloroethylene and water, for example, bearing in mind that $T_1 \simeq T_2$, [21] gives $(MW)_{tr}/(MW)_w \simeq 1.9$. If the gas used with water is air (mean molecular weight about 29) the gas used with trichloroethylene must have a mean molecular weight of the order of 55, which is quite feasible. The required dynamic viscosity however is about 0.56 times that of air which would be difficult or impossible to realise in a gas mixture of the correct density. Choice of a gas with a higher viscosity than air (e.g. neon, argon) would remove this problem.

In practice, given the validity of the criteria, satisfaction of [16] may often be unimportant since the influence of μ_G' in the various two-phase phenomena will often be very slight (e.g. in bubbly flow). In this case the only severe restriction is equality of Q for the liquids used. Tests of the similarity of water and trichloroethylene two-phase flows which satisfy the above similarity criteria are now being set up at Delft University of Technology for case of vertical upward pipe flow and a wide range of flow types from bubbly to annular mist.

4. VALIDITY OF THE CONVENTIONAL PHYSICAL MODEL

The assumptions underlying the conventional physical model are the following:

(1) a surfactant-free, incompressible, Newtonian liquid
(2) a perfect, Newtonian gas
(3) no mass transfer between the phases
(4) isothermal flow
(5) no velocity discontinuity at the interface
(6) no influence of liquid–solid contact angle, i.e. solid walls either totally wet or totally dry
(7) no special effects present during the rupture of thin films or filaments of either phase.

These will be considered in turn to see to what extent they can be realised in actual flows.

In most types of flow, sufficient purity of the liquid can be achieved to render the effects of surface active agents negligible. The treatment of many liquids as incompressible and Newtonian is of course accurately justified, so assumption (1) is valid in many situations.

Assumption (2) is a good approximation for most gases if the vapour content is low. The saturated vapour pressure of most liquids is only a few percent of the absolute pressure if they are of the order of 100°C from their boiling points. Under these circumstances, therefore, assumption (2) is justifiable, as is assumption (3).

Strictly, a contradiction exists between pressure variation in a gas flow and isothermal conditions [assumption (4)]. However, because large pressure variations are usually accompanied by high velocities and increased inter-dispersion of the phases, and because the heat capacity of the liquid phase is usually much greater than that of the gas, the isothermal approximation should nevertheless be a good one in many flows. A small departure from isothermal conditions which might not, however, have negligible consequences could occur in the final stages of thinning of liquid films or filaments. Here the increase of surface area per unit volume leads to a cooling of the film (filament) which, though offset by conduction from the neighbouring fluid increases the surface tension locally and so decreases the thinning rate, as occurs with surface active agents. According to Lee (1973) this can be a decisive effect in some bubble coalescence situations. This represents the first of the possible "special effects" mentioned in assumption (7).

As with the similar no-slip condition at a solid boundary, assumption (5) should be justified for all but highly rarefied gas flows. Assumption (6) is valid in many flows and where it is not, the influence of contact angle will often be negligible.

For flows with joining or dividing phase boundaries (coalescing bubbles or droplets, atomising liquids or gases) the final thinning mechanics of the relevant films or filaments must be taken into account in any complete description of the flow. The possibility of non-negligible thermal effects has been mentioned. Other special effects are the emergence of inter-molecular attractive forces not adequately described by a simple surface tension, such as the van der Waals pressure, and the breakdown of the continuum description altogether when the film or filament becomes very thin.

If any of these effects produces an appreciable delay or acceleration of the final thinning process it will manifest itself in the rate of development of the whole flow and the similarity criteria based on the conventional physical model will not apply. Since no general estimate of the magnitude of these effects is available the similarity criteria derived above must at present be regarded as suspect on the grounds of assumption (7) except for "separated" gas–liquid flows where each phase is continuous and remains so.

In what follows the van der Waals pressure is examined in more detail and a first attempt made to estimate its influence on the thinning time of liquid films.

5. THE VAN DER WAALS PRESSURE IN THIN FILMS

Attractive "van der Waals" forces arise between all molecules. Their magnitude depends greatly on the molecule concerned and falls off steeply with distance. Because of their very short range their effects are confined to a surface layer and can normally be represented by a surface tension. In very thin liquid films, however, ($\leqslant 10^{-7}$ m) the whole film becomes a part of the surface layer. Molecules in a thinner part of the film are less tightly bound and a tendency therefore exists for liquid to flow from thin to thick which can be expressed, energetically, as the existence of an additional compressive force on the film, the "van der Waals pressure", Π. The magnitude of this pressure is in fact independent of whether the film is one of liquid in gas or gas in liquid and for films of the order of 10^{-7} m or less is given by

$$\Pi = A/6\pi h^3 \qquad [22]$$

(Hamaker 1937; Verwey & Overbeek 1948; Scheludko 1962). Here h is the film thickness and A, the Hamaker constant, depends on the liquid (and, in principle, on the gas too).

Because of its h^{-3} dependence, once Π becomes comparable with the conventional stresses responsible for thinning of the film, thinning will accelerate and rupture rapidly follow. The sequence of events is depicted in figure 1. (a) and (b) represent two flows satisfying the simple similarity criteria which therefore have the same normalized thinning curve up to the point that the van der Waals pressure becomes important. Thereafter the liquid with relatively stronger van der Waals forces thins more rapidly and $\Delta t'$ represents the resulting difference in normalized rupture time. If $\Delta t'$ is comparable with the time required for significant change in the main flow then a noticeable non-similarity of the two flows will result and the simple criteria will not suffice.

To estimate $\Delta t'$ in the cases treated below, thinning will be treated as following the conventional model down to a critical thickness h_c' (figure 1), at which the film abruptly ruptures. An estimate of h_c' will be obtained from the thickness at which the van der Waals pressure Π becomes equal to the conventional stress responsible for thinning. The h_c' so obtained is a

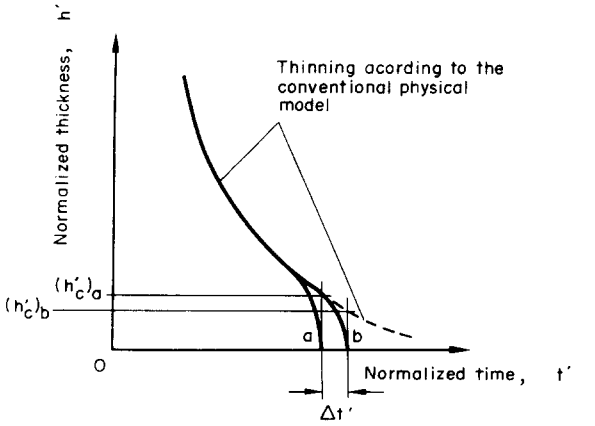

Figure 1. Thinning of a film with (a) relatively strong van der Waals forces, (b) relatively weak.

function of the Hamaker constant A, and typical variations in A can be translated into variations in h'_c and thence, via the conventional thinning equation found, into typical variations in the rupture time, $\Delta t'$.

6. THINNING MODEL FOR THE FILM BETWEEN EQUAL COALESCING BUBBLES

The sequence of events leading to bubble coalescence may in general be expected to be as follows:

(1) For reasons associated with the main flow the bubbles attain a relative approach velocity, resulting in a flow of liquid away from the zone between them.

(2) Because of the inertia of this flow the bubble centres continue to approach each other even when the pressure required to produce this flow becomes of the order of the capillary pressure, and flattening of the adjacent surfaces (film formation) occurs.

(3) As the bubble centres continue to approach each other the film grows in diameter while at the same time outward flow within it reduces its thickness.

(4) When part of the film becomes sufficiently thin, the van der Waals pressure becomes important and rupture rapidly follows.

The model used to estimate the thinning rate of the film is that of a parallel sided film of fixed radius, a, later taken to be the mean radius during the whole process (figure 2). The most serious approximation here is probably that of parallel sidedness. In reality such a film would rapidly develop the dimpled form indicated in figure 3 and observed in films with immobile interfaces (MacKay & Mason 1963). This means not only that the capillary driving pressure at the film centre is greater than in a parallel film, but also that the amount of liquid which must be expelled to permit any given minimum thickness to be reached is much less. Consequently the estimated final thinning rate in the present analysis is likely to be conservative (these conclusions are borne out by preliminary results of finite-difference calculations now in progress) leading to an exaggerated estimate of the influence of van der Waals forces on the rupture time.

Thinning of a parallel sided, constant radius film

The situation is illustrated in figure 2. It is assumed that gas shear and pressure variation are negligible and that:

$$b \sim a \qquad [23]$$

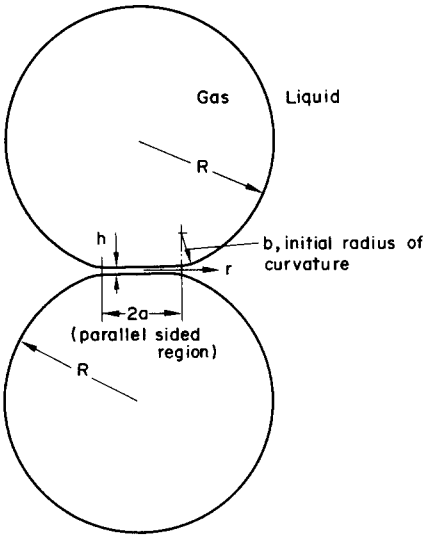

Figure 2. Model of coalescing bubbles.

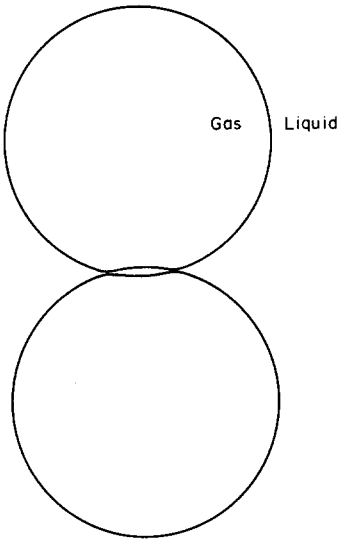

Figure 3. Dimpled film between coalescing bubbles.

$$h \ll a \ll R, \tag{24}$$

$$g\rho_L a \ll 2\sigma/R, \tag{25}$$

where unprimed symbols now denote original, dimensional quantities. Assumption [24] permits transverse gradients and velocity components to be neglected. [25] permits gravity to be neglected. Both assumptions are examined later.

Continuity gives

$r \leq a$

$$u = -\frac{r}{2h} \cdot \frac{dh}{dt} = -r\frac{dH}{dt}, \tag{26}$$

$a \leq r \ll b$

$$u = \frac{-r}{[1+(r-a)^2/bh]} \cdot \frac{dH}{dt}, \tag{27}$$

where $H = \frac{1}{2} \ln h$.

Substituting [26] into the Navier–Stokes equation for the radial direction and integrating with respect to r from 0 to a:

$$p_a = p_0 - \frac{\rho a^2}{2}\left[\left(\frac{dH}{dt}\right)^2 - \frac{d^2H}{dt^2}\right] \tag{28}$$

where the subscript L is now omitted.

Integrating likewise for the region $r = a$ to $r = a + kb$:

$$p_a = -\rho\frac{d^2H}{dt^2}\left[\frac{\pi a\sqrt{(bh)}}{2} + \frac{bh}{2}\ln\left(\frac{k^2b}{h}\right)\right] - \rho\left(\frac{dH}{dt}\right)^2\left[\frac{a^2}{2} + bh\ln\left(\frac{k^2b}{h}\right) - bh + \frac{\pi a\sqrt{(bh)}}{2}\right] - 2\mu\frac{dH}{dt}, \tag{29}$$

where k is less than but of the order of unity so that transverse terms may still be neglected at the outer limit and yet the velocity and pressure can be approximated as zero.

Equating the right hand sides of [28] and [29] the terms containing b are found to be negligible in view of [23] and [24] provided

$$\left(\frac{dH}{dt}\right)^2 \leq \left|\frac{d^2H}{dt^2}\right| \text{ or } \left|\frac{4\mu}{\rho a^2}\frac{dH}{dt}\right|. \quad [30]$$

It is seen later that [30] is fulfilled. The following equation is then obtained

$$\frac{d^2H}{dt^2} + \frac{4\mu}{\rho a^2}\cdot\frac{dH}{dt} + \frac{2p_0}{\rho a^2} = 0. \quad [31]$$

p_0 is related to $(P_0)_L$, the normal stress at the film centre by

$$\begin{aligned}(P_0)_L &= -p_0 + 2\mu\left(\frac{\partial w}{\partial z}\right)_0 \\ &= -p_0 - 4\mu\left(\frac{\partial u}{\partial r}\right)_0 \text{ by continuity} \\ &= -p_0 + 4\mu\frac{dH}{dt}\end{aligned} \quad [32]$$

from [26]. Further,

$$(P_0)_L = (P_0)_G = -p_G = -2\sigma/R. \quad [33]$$

Substituting in [32],

$$p_0 = \frac{2\sigma}{R} + 4\mu\left(\frac{dH}{dt}\right). \quad [34]$$

Substituting in [31], the thinning equation of the film is obtained:

$$\frac{d^2H}{dt^2} + \frac{12\mu}{\rho a^2}\cdot\frac{dH}{dt} + \frac{4\sigma}{\rho a^2 R} = 0. \quad [35]$$

This can be integrated to give

$$\frac{dH}{dt} = \left[\frac{\sigma}{3\mu R} + \left(\frac{dH}{dt}\right)_0\right]\exp(-12\mu t/\rho a^2) - \frac{\sigma}{3\mu R} \quad [36]$$

and again to give

$$H_0 - H = -\frac{\rho a^2}{12\mu}\left[\frac{\sigma}{3\mu R} + \left(\frac{dH}{dt}\right)_0\right][1 - \exp(-12\mu t/\rho a^2)] + \frac{\sigma t}{3\mu R}. \quad [37]$$

If

$$\frac{4\mu}{\rho a^2}\cdot t \ll 1 \text{ and } \left|\frac{3\mu R}{\sigma}\cdot\left(\frac{dH}{dt}\right)_0\right| \ll 1, \quad [38]$$

an expansion of the exponential indicates that the terms containing μ may be neglected.

Thinning is then inertia-controlled and [37], [36], [35] and [34] become respectively

$$t = \frac{\rho a^2 R}{4\sigma}\left(\frac{dH}{dt}\right)_0\left[1-\left\{1+8\sigma(H_0-H)/\rho a^2 R\left(\frac{dH}{dt}\right)_0^2\right\}^{1/2}\right], \quad [39]$$

$$\frac{dH}{dt} = \left(\frac{dH}{dt}\right)_0 - \frac{4\sigma}{\rho a^2 R}t, \quad [40]$$

$$\frac{d^2H}{dt^2} = -\frac{4\sigma}{\rho a^2 R}, \quad [41]$$

$$p_0 = 2\sigma/R. \quad [42]$$

Henceforth considerations will be confined to this situation which will later be seen to include many coalescence situations in low viscosity liquids such as water.

Typical film radius and initial conditions

In order to make use of the thinning equation [39], values are needed for the initial conditions h_0 and $(dH/dt)_0$ and for the mean film radius. An estimate of h_0 can be obtained from the separation at which the pressure generated between approaching spherical bubbles becomes sufficient to cause appreciable deformation

$$\text{e.g.} \quad p_0 = \sigma/R. \quad [43]$$

An expression for p_0 is obtained from [29] taking $a = 0$, $b = R$ and $-(dh/dt) = V$, the bubble approach velocity (assumed constant):

$$p_0 = \frac{\rho V^2 R}{4h_0}\left(1+\frac{4\mu}{\rho VR}\right). \quad [44]$$

In bubbly flows coalescence of equal bubbles occurs by one bubble wholly or partially entering the wake of the preceeding one. V may therefore be expected to be an order of magnitude less than the velocity with which the bubbles travel with respect to the liquid. In pressure gradients less than or of the order of g, this latter velocity will be of the order of the rise velocity of the bubbles in still liquid. For low-viscosity liquids such as water, the rise velocity is of the order of 20 cm sec^{-1} for bubbles of 1 mm dia or more (Brodkey 1967), giving $V \simeq 2$ cm sec^{-1}. The corresponding values of the viscous term in [44] are small (≤ 0.1 if $R \geq 2$ mm) and will be neglected:

$$\frac{4\mu}{\rho VR} \ll 1. \quad [45]$$

It will shortly be seen that [45] justifies the assumption that thinning is inertia controlled.

Incorporating [45], [43] and [44] give

$$\frac{h_0}{R} = \frac{\rho V^2 R}{4\sigma}, \quad [46]$$

and

$$\left(\frac{dH}{dt}\right)_0 = \frac{1}{h_0}\left(\frac{dh}{dt}\right)_0 = -\frac{V}{h_0} = -\frac{2\sigma}{\rho VR^2}. \quad [47]$$

h_0 is seen to be very small in relation to R. For example, for water at 20°C, $R = 2$ mm and $V = 2$ cm sec^{-1}, $h_0/R = 1/365$. The radius of the film, a, may therefore be approximated by the

value which would result if the bubbles were spherical and in contact at $t = 0$ and their centres continued to approach each other at the velocity V. In view of [24] this is given by

$$a^2 = 2RVt,$$

and the mean of a over a period t is

$$a = (8RVt/9)^{1/2} \simeq (RVt)^{1/2}. \qquad [48]$$

If [47] and [48] are substituted in [39] the thinning equation becomes

$$t = \frac{\rho V R^2}{4\sigma}(H_0 - H), \qquad [49]$$

or

$$t' = \frac{W}{4}(H_0' - H'), \qquad [50]$$

where t' and H' are the normalized quantities tV/R and $\frac{1}{2}\ln(h/R)$ respectively and W is the Weber number $\rho V^2 R/\sigma$. In the present context t' is chosen as the time of rupture so that

$$H_0' - H' = \ln(h_0'/h_c')^{1/2}, \qquad [51]$$

where h_c' is the effective rupture thickness discussed in section 5 and represented in figure 1.

Justification of the assumptions of the model

The various assumptions made during the derivation of the thinning equation can now be examined. From [46], [48] and [50]

$$a/R = [W(H_0' - H')/4]^{1/2}, \qquad [52]$$

$$h_0/a = [W/4(H_0' - H')]^{1/2}, \qquad [53]$$

$$\frac{g\rho a}{(2\sigma/R)} = \frac{g\rho R^2}{2\sigma}[W(H_0' - H')/4]^{1/2}. \qquad [54]$$

For the assumptions [24] and [25] to apply, the left hand sides of [52], [53] and [54] must be considerably smaller than unity. From [51], H_0'–H' is of the order of unity and a typical value will be seen to be 3. Taking this value, $V = 2$ cm sec^{-1} and water at 20°C, [52], [53] and [54] yield the following values:

R(mm)	a/R	h_0/a	$g\rho a/(2\sigma/R)$
0.5	0.045	0.002	0.001
2	0.09	0.003	0.023
5	0.14	0.005	0.22
20	0.28	0.010	7.2

The assumptions are thus approximately satisfied for bubbles of 5 mm radius or less.

Making use of [47], [48], [49], [40] and [41] the first alternative of assumption [30] reduces to

$$\frac{9}{4}(H_0' - H') \lesssim 1,$$

which is just satisfied remembering that $H_0' - H' \simeq 3$.

Finally, making use of [48] and [47], assumption [38], justifying the use of the inertia-controlled thinning expression, becomes

$$\frac{4\mu}{\rho VR} \ll 1 \text{ and } \frac{6\mu}{\rho VR} \ll 1,$$

which has already been shown to be satisfied for bubbles of a few mm dia or more in low-viscosity liquids such as water [45].

In summary, therefore, the inertia-controlled thinning equation [49] or [50] should be a good approximation for bubbles between 1 mm and 10 mm dia in low-viscosity liquids such as water, apart from the parallel-film assumption which under-rates the final thinning rates.

7. INFLUENCE OF VAN DER WAALS PRESSURE ON THE INSTANT OF COALESCENCE

As discussed in section 5, an estimate of the effective normalized rupture thickness h'_c may be obtained from the thickness at which the van der Waals pressure Π becomes equal to the corresponding stress responsible for thinning. In the present case this stress will be taken as the pressure difference between the centre and the edge of the parallel film: $p_0 - p_a$ (p_a is negative relative to the pressure in the bulk of the liquid). h'_c is then given by $\Pi = p_0 - p_a$.

$$\text{i.e. } \frac{A}{12\pi h_c'^3} = R^2\sigma\left[1 + \frac{9}{8}\ln\left(\frac{W}{4h'_c}\right)\right] \qquad [55]$$

making use of [22] and [28] and the appropriate expressions for a, (dH/dt) and (d^2H/dt^2). h'_c can be found from [55] by trial and error.

To observe the influence of the Hamaker constant A on the value of h'_c consider the liquids water and aniline for which Scheludko (1962) found $A = 7 \times 10^{-20}$ and 7×10^{-19} kg m^{2}sec^{-2} respectively. These two liquids satisfy the similarity requirement of equal Q (section 3) if the water is at 20°C and the aniline at somewhat less than 10°C (when $\rho_{an} \simeq 1.03 \times 10^3$ kg m^{-3}, $\sigma_{an} \simeq 43 \times 10^{-3}$ kg sec^{-2}, $\mu_{an} \simeq 0.68 \times 10^{-3}$ kg m^{-1} sec^{-1}). The required ratio of bubble radii for dynamically similar coalescence is found from [18] to be $R_{an}/R_w = 0.755$.

Choosing $V_w = 2$ cm sec^{-1} and $R_w = 2$ mm, which is in the middle of the range of validity of the thinning model, [55] gives

$$(h'_c)_w = 0.99 \times 10^{-5} \; (h_c = 198 \text{ Å}, H'_0 - H' = 2.8)$$

$$(h'_c)_{an} = 3.2 \times 10^{-5} \; (h_c = 480 \text{ Å}).$$

The corresponding difference in the normalized rupture times in the two flows is given by [50] and [51]:

$$t'_w - t'_{an} = \frac{W}{4}[\ln(h'_0/h'_c)_w^{1/2} - \ln(h'_0/h'_c)_{an}^{1/2}]$$

$$= \frac{W}{8}\ln[(h'_c)_{an}/(h'_c)_w] \qquad [56]$$

since $(h'_0)_{an} = (h'_0)_w = W/4$ from [46]. In the present case [56] gives $t'_w - t'_{an} = 1.6 \times 10^{-3}$. This corresponds to a real-time interval of 1.6×10^{-3} R/V: 1.6×10^{-4} sec. That is, rupture occurs 1.6×10^{-4} sec later in the water flow than it would if it were truly dynamically similar to the aniline flow. Bearing in mind that the final thinning rate estimated by the parallel-film model is conservative, the actual time interval would be less.

In typical flows of a few msec^{-1} this delay, equivalent to the order of 0.1 mm or less in

distance would probably be undetectable and the conclusion is therefore that the dynamic similarity criteria should apply accurately except insofar as thermal effects are of influence (section 4). As R increases the delay increases approximately as R^2. If this trend continues beyond the range of validity of the present model (R = 5 mm), the delay could become significant for bubbles of a few cm dia. Whether or not this is so depends on the extent to which dimpling of the film accelerates final thinning. Calculations of the thinning of actual, dimpled films are therefore of considerable interest.

8. THINNING MODEL OF AN ATOMISING LIQUID SHEET

A liquid sheet injected into still gas exhibits the classical Kelvin–Helmholtz instability and develop waves after which atomisation generally occurs. For thin sheets (thickness, $h \ll$ wavelength, λ) these are predominantly of the sinuous type while for thick sheets dilational waves are also possible (figure 4). The initial instability has been studied theoretically for the inviscid case (Squire 1953; Haggerty & Shea 1955; Dombrowski & Hooper 1961; Dombrowski 1962; Clark & Dombrowski 1972; Crapper *et al.* 1973) but in the case of sinuous waves the mechanism of rupture is still obscure. On the one hand without the waves, as in the case of low gas pressure, rupture is greatly delayed and finally occurs via thread formation at the sheet edge (Dombrowski & Hooper 1961) and on the other hand the intrinsic stretching of the sheet due to the waves is too slight to explain rupture.

The explanation clearly lies in unequal thinning within each wave due to some additional mechanism. Clark & Dombrowski (1972) have indicated one such mechanism: a second order dilational harmonic which, if its growth continued in the initial exponential way, would cause rupture in the correct order of distance. The validity of this analysis is restricted to the very early stages of growth, however, so that as regards the final thinning rate nothing can safely be concluded, quite apart from the neglect of viscous effects.

The present analysis is mainly concerned with the final thinning rates. The existence of developed waves is taken for granted and the variation of the gas normal and tangential stresses over a wave examined. Both types of variation are seen to exist and to lead to local thinning (normal-stress or pressure thinning is probably equivalent to Clark and Dombrowski's second order harmonic) but tangential-stress or shear thinning dominates in the final stages.

Pressure thinning

The Kelvin–Helmholtz instability originates in the underpressure generated when the gas flows over a wave crest combined with an overpressure on the other side of the sheet where a trough exists. For small amplitude waves the magnitudes of the under and overpressures are almost equal, but for moderate amplitudes the underpressure is markedly greater. This is shown by Motzfeld's measurements (Ursell 1956) on the non-separated flow over the last of three wooden sine waves (figure 5). For the smaller amplitude, $a/\lambda = 1/40$, the under and overpressure are almost equal, but for $a/\lambda = 1/20$ the underpressure is almost twice as great (a, wave amplitude).

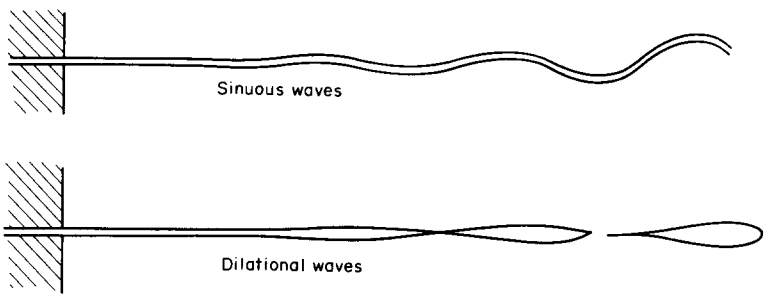

Figure 4. Sinuous and dilational instabilities of a moving liquid sheet.

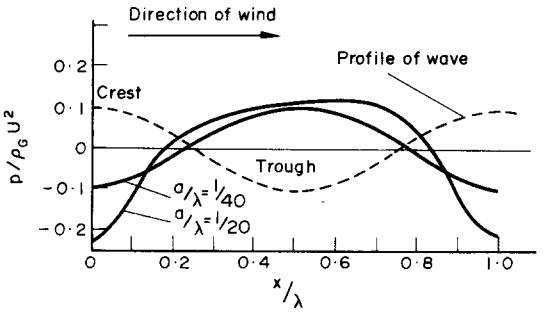

Figure 5. Gas-pressure variation over a sine wave (Motzfeld).

The related variation of static pressure within the liquid sheet is readily derived, treating the liquid as inviscid for the present. Referring to figure 6, the mean pressure, p, within any section of the sheet is given by

$$\begin{aligned} p &= (p_{A'} + p_{B'})/2 \\ &= (p_A + \sigma/R_A + p_B - \sigma/R_B)/2 \\ &\simeq (p_A + p_B)/2 , \end{aligned}$$

since $R_A \simeq R_B$ as $h \ll \lambda$. Here A and A', B and B' are points on the gas and liquid sides of the interface respectively. Since p_B is also the gas pressure $\lambda/2$ away from A on the same side of the sheet, Motzfeld's results can be converted into a variation of p within an equivalent sheet. The resulting variation is shown in figure 7 for the case $a/\lambda = 1/20$. The pressure is a minimum at a crest (/trough) and a maximum between crests (/troughs) and will therefore produce a flow of liquid towards the crests (/troughs) and cause local thinning between them.

To estimate the resulting thinning rate, parallel sided thinning will first be considered, still treating the liquid as inviscid. Suppose the imposed pressure is symmetrical with a maximum at $x = 0$ (where x represents distance in the direction of motion of the sheet). Symmetry and continuity then give

$$u = -\frac{x}{h}\frac{dh}{dt} = -x\frac{dH}{dt} , \qquad [57]$$

where $H = \ln h$ now. Neglecting the influences of gravity, transverse acceleration of the sheet

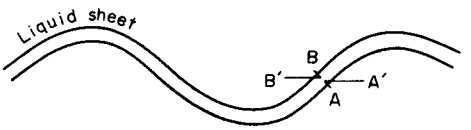

Figure 6. Sinuous sheet.

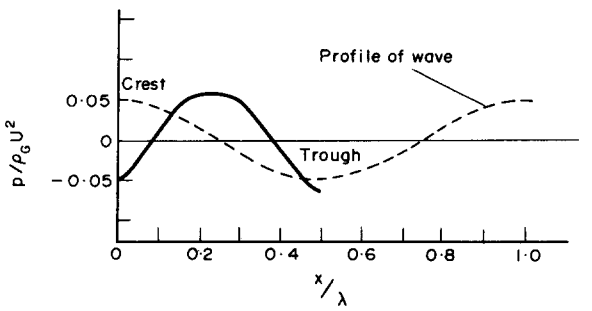

Figure 7. Mean-pressure variation within a sinuous sheet.

and transverse gradients and components of velocity within the sheet, the Navier–Stokes equation for the x-direction is

$$-\frac{1}{\rho}\frac{\partial p}{\partial x}=\frac{\partial u}{\partial t}+u\frac{\partial u}{\partial x}$$

$$=x\left[\left(\frac{\mathrm{d}H}{\mathrm{d}t}\right)^2-\frac{\mathrm{d}^2H}{\mathrm{d}t^2}\right]$$

from [57]. Integrating with respect to x

$$p=p_0-\frac{\rho x^2}{2}\left[\left(\frac{\mathrm{d}H}{\mathrm{d}t}\right)^2-\frac{\mathrm{d}^2H}{\mathrm{d}t^2}\right]. \qquad [58]$$

The required pressure distribution for parallel sided thinning is thus a quadratic one. But any pressure distribution is quadratic close to a maximum since, by a Taylor expansion

$$p=p_0+x\left(\frac{\partial p}{\partial x}\right)_0+\frac{x^2}{2}\left(\frac{\partial^2 p}{\partial x^2}\right)_0+0(x^3), \qquad [59]$$

and $(\partial p/\partial x)_0$ is zero. Equating the coefficients of x^2 in [58] and [59], the thinning equation at the maximum-pressure point of the sheet is obtained:

$$\left(\frac{\mathrm{d}H}{\mathrm{d}t}\right)^2-\frac{\mathrm{d}^2H}{\mathrm{d}t^2}=-\frac{1}{\rho}\left(\frac{\partial^2 p}{\partial x^2}\right)_0. \qquad [60]$$

An estimate of $(\partial^2 p/\partial x^2)_0$ can be obtained by approximating the variation of p (figure 7) by a cosine curve of wavelength $\lambda/2$:

$$p=p_0\cos\left(\frac{4\pi x}{\lambda}\right),$$

$$\left(\frac{\partial^2 p}{\partial x^2}\right)_0=-\frac{16\pi^2}{\lambda^2}p_0=-\frac{16\pi^2}{\lambda^2}\cdot\alpha\rho_G U^2, \qquad [61]$$

where the coefficient α can be expected to be a function primarily of a/λ and is about 0.05 for Motzfeld's case of $a/\lambda = 1/20$ (figure 7).

Substituting [61] into [60] the pressure-thinning equation is obtained:

$$\left(\frac{\mathrm{d}H}{\mathrm{d}t}\right)^2-\frac{\mathrm{d}^2H}{\mathrm{d}t^2}=\frac{16\pi^2\alpha\rho_G U^2}{\rho_L\lambda^2}. \qquad [62]$$

Shear-thinning

A realistic assessment of the shear stress variation over the surface of a wave is more difficult than that of the pressure variation. Considering again non-separated flow, two factors will be of influence. The first is a growth of the mean boundary layer from origin onwards, determining the mean shear stress (figure 8). The second is the acceleration of the boundary layer at each crest by the local underpressure causing a high local shear stress, and the converse phenomenon at each trough (figure 9).

As seen from figure 5, the underpressure created at the crest is about 50 per cent of the gas dynamic pressure for $a/\lambda = 1/20$. Non-separated flow over the waves appears to continue to

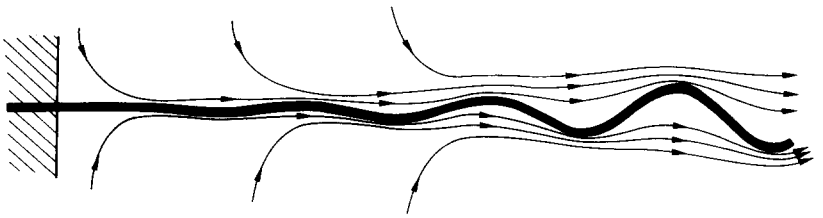

Figure 8. Growth of the gas boundary layer on a sinuous sheet.

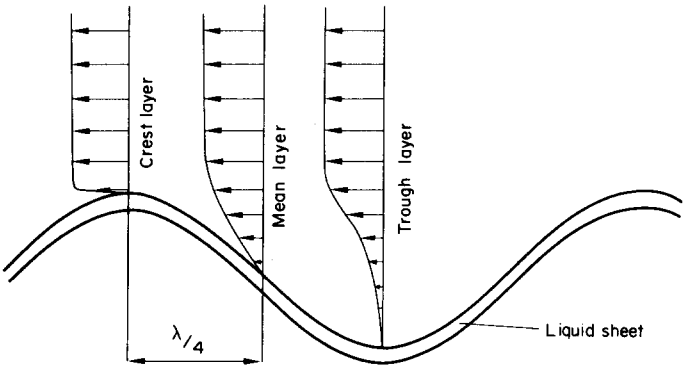

Figure 9. Variation of the boundary layer over a wave (viewed with respect to the sheet).

values of a/λ of the order of 1/10 (Crapper *et al.* 1973) at which stage the underpressure may be expected to excede the gas dynamic pressure. Typically therefore, the boundary layer will be accelerated from its mean condition (corresponding to zero underpressure) to the order of the mainstream velocity U in a distance of $\lambda/4$. The resulting crest shear stress, τ_0, should therefore be comparable to that on a flat plate at a distance $\lambda/4$ from its leading edge:

$$\tau_0 \sim \frac{\rho_G U^2}{3} \sqrt{\left(\frac{4\mu_G}{\rho_G U \lambda}\right)}. \qquad [63]$$

The shear stress due to the mean boundary layer is approximately given by a similar expression with $\lambda/4$ replaced by the distance from origin and is therefore much smaller than τ_0. At the troughs the shear stress is smaller still. The total shear stress τ (including both sides of the sheet) may therefore be expected to vary in the manner shown in figure 10 and can be approximated by the equation

$$\tau = \tfrac{1}{2}\tau_0[1 + \cos(4\pi x/\lambda)]. \qquad [64]$$

The variation of τ over a wave will produce unequal deceleration of the different parts of the sheet, resulting in a stretching and thinning of some zones and a compression and thickening of others. The thinning is readily analysed if shearing motion within the sheet itself is neglected (i.e.

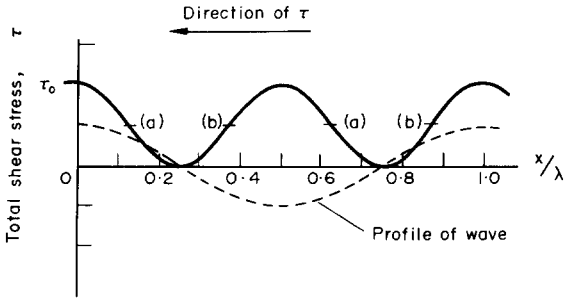

Figure 10. Variation of the total shear stress over a wave.

if "plug flow" is assumed). This can be shown to be well justified even for low-viscosity liquids provided the sheet thickness is less than about 10^{-3} cm. Thicknesses in the final stages of thinning are several orders of magnitude less than this and the force due to τ can then be replaced by that due to an equivalent pressure gradient

$$\frac{\partial p}{\partial x} = -\frac{\tau}{h}. \qquad [65]$$

This pressure gradient has a strength proportional to $1/h$ and consequently becomes dominant over conventional pressure thinning in the final stages of thinning.

A similar analysis to that for pressure thinning yields the equation for parallel sided shear thinning

$$\frac{1}{\rho h}\frac{\partial \tau}{\partial x} = \left(\frac{dH}{dt}\right)^2 - \frac{d^2H}{dt^2}. \qquad [66]$$

Differentiating with respect to x,

$$\frac{\partial^2 \tau}{\partial x^2} = 0 \qquad [67]$$

which is evidently a necessary condition for parallel sided thinning as well as the condition that the thinning rate, governed by $\partial\tau/\partial x$, be a maximum or a minimum. [67] is satisfied at the inflexion points (a) and (b) (figure 10) where the thinning rate is respectively a maximum and a minimum (i.e. maximum thickening rate).

Substituting in [66] from [64] and [63],

$$\left(\frac{dH}{dt}\right)^2 - \frac{d^2H}{dt^2} = \frac{4\rho_G U^2}{\rho_L h\lambda}\sqrt{\left(\frac{\mu_G}{\rho_G U\lambda}\right)}. \qquad [68]$$

This is the same as the pressure-thinning equation [62] apart from the right hand term representing the driving force. Equating the right hand terms, the two types of thinning are seen to be equally powerful if

$$h = \frac{1}{4\pi^2\alpha}\sqrt{\left(\frac{\mu_G\lambda}{\rho_G U}\right)}. \qquad [69]$$

Below this value of h shear thinning dominates since the right hand side of [68] varies as h^{-1} whereas the right hand side of [62] is constant.

To evaluate [69], estimates of α and λ are required. α was seen to be 0.05 for $a/\lambda = 1/20$ and to increase rapidly with increasing a/λ. Since, however, a maximum value of a/λ of about 1/10 is imposed by the occurrence of flow separation a typical value of α in the non-separated regime will be taken as 0.1. An indication of the value of λ is given by the mostly rapidly amplified wavelength according to inviscid theory:

$$\lambda_{max} = 4\pi\sigma/\rho_G U^2. \qquad [70]$$

Observed values of λ are higher, though of the same order (Clark & Dombrowski 1972), and a typical value will be taken to be $2\lambda_{max}$. [69] then becomes

$$h = \frac{10}{\rho_G}\sqrt{\left(\frac{\mu_G\sigma}{2\pi^3 U^3}\right)}. \qquad [71]$$

For the case of water and air at atmospheric pressure and 20°C with $U = 20$ m sec^{-1}, [71] gives $h = 1.4 \times 10^{-3}$ cm. As noted earlier, values of h in the final stages of thinning are several orders of magnitude smaller than this and it is therefore clear that shear thinning will dominate completely.

Taking the initial thinning rate, $-(dh/dt)$, to be zero the shear thinning equation [68] can be integrated with respect to t to give

$$\frac{dh}{dt} = -[Bh\{1-(h/h_0)^3\}]^{1/2}, \qquad [72]$$

where

$$B = \frac{8\rho_G U^2}{3\rho_L \lambda}\sqrt{\left(\frac{\mu_G}{\rho_G U \lambda}\right)}. \qquad [73]$$

For $h \ll h_0$, as is the case during the final stages of thinning, [72] becomes

$$\frac{dh}{dt} = -(Bh)^{1/2}. \qquad [74]$$

Integrating again,

$$\Delta t = -2B^{-1/2}\Delta(\sqrt{h_c}) \qquad [75]$$

where Δt is the variation in rupture time associated with variations in the effective rupture thickness h_c.

The influences of flow separation and of liquid viscosity

The preceeding analysis is for non-separated gas flow and negligible liquid viscosity except insofar as it is required to justify the "plug flow" model of the film. In reality, flow separation does occur when the amplitude of the waves becomes sufficient (Crapper & Dombrowski 1973) and liquid viscosity must provide some resistance to the deformation involved in the stretching and thinning of the film.

The effect of flow separation is to limit the pressure variation which can occur over a wave. The general form of the pressure variation will not be greatly altered and expression [62] for pressure thinning should still be roughly valid, with the coefficient α of the same order as for non-separated flow. The crest shear stress τ_0 should likewise remain of the same order as before, but the occurrence of a stagnation point P (figure 11) means that the local shear stress gradient and hence, from [66], the shear thinning rate are theoretically infinite. In reality the position of P probably fluctuates but a pronounced increase in the thinning rate in this zone (which is also the original zone of maximum thinning) probably results. Once again, therefore, the present estimate of the final thinning rate is likely to be conservative, leading to an exaggerated estimate of the influence of van der Waals forces on the rupture time.

An estimate of the importance of liquid viscosity can be obtained from the underpressure created in the maximum thinning zone as a consequence of the deformation there:

$$\left.\begin{aligned} p &= -P + 2\mu_L \frac{\partial w}{\partial z} \\ &= -P - 2\mu_L \frac{\partial u}{\partial x} \\ &= -P + 2\mu_L \frac{dH}{dt} \\ &= -P - 2\mu_L (B/h)^{1/2} \end{aligned}\right\} \text{ by continuity}$$

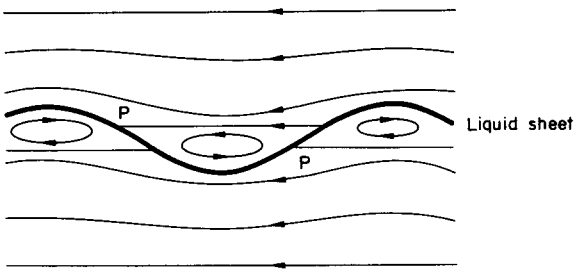

Figure 11. Separated flow over a wave.

assuming the thinning rate to be approximately given by the inviscid expression [74]. Here p is the pressure at any point in the sheet and P the stress normal to the plane of the sheet. P is related to the external gas pressure via the transverse acceleration of the sheet and the normal-stress interface condition. The term $-2\mu_L(B/h)^{1/2}$ is an additional underpressure caused by liquid viscosity and will tend to produce pressure thickening. Its importance can be gauged by comparing it with the pressure variation over the thinning zone which is equivalent to the shear stress:

$$\Delta p = \frac{\partial p}{\partial x} \cdot \Delta x \sim \frac{\tau_0}{h} \cdot \frac{\lambda}{8} \qquad [76]$$

from [65], $\lambda/8$ being the half-width of the zone. The viscous term is thus negligible if $2\mu_L(B/h)^{1/2} \ll (\tau_0/h) \cdot (\lambda/8)$.

Making use of [63] and [73] and taking $\lambda = 2\lambda_{max}$ again ([70]), this condition becomes

$$h \ll \frac{\pi^3\sigma^3\rho_L}{3(\mu_L\rho_G U^2)^2}\sqrt{\left(\frac{\mu_G U}{8\pi\sigma}\right)}. \qquad [77]$$

For water and air at atmospheric pressure and 20°C with $U = 20$ m sec^{-1}, [77] yields $h \ll 25$ cm. The effect of viscosity is thus entirely negligible, and would become important in the final stages of thinning only for liquids with $\mu_L \gtrsim 1000\,\mu_{water}$.

9. INFLUENCE OF VAN DER WAALS PRESSURE ON THE BREAKUP TIME

Once again, an estimate of the effective rupture thickness h_c is obtained from that at which the van der Waals pressure, Π, becomes equal to the corresponding stress responsible for thinning, in this case the equivalent pressure variation over the thinning region, Δp, as derived in [76]:

$$\Pi = \Delta p. \qquad [78]$$

Making use of [22], [76] and [63] and taking $\lambda = 2\lambda_{max}$, [78] yields

$$h_c^2 = \frac{A}{\pi\sqrt{2\pi\sigma\mu_G U}}. \qquad [79]$$

The values of h_c may now be calculated for water and aniline flows satisfying the simple similarity criteria of sections 2 and 3. Taking the water situation as water in air at atmospheric pressure and 20°C with $U = 20$ m sec^{-1}, [79] yields $(h_c)_w = 1.3 \times 10^{-9}$ m (13 Å). The corresponding values of U and μ_G for the aniline flow are given by [17] and [16], and [79] then yields

$$(h_c)_{an} = 5.4 \times 10^{-9} \text{ m (54 Å)}.$$

Strictly speaking, continuum theory no longer applies at such thicknesses but the thinning equation should nevertheless predict the correct order of variation in the rupture time.

The normalized rupture thicknesses, h'_c, bear the ratio

$$\frac{(h'_c)_w}{(h'_c)_{an}} = \frac{(h_c)_w}{(h_c)_{an}} \times \frac{(x_C)_{an}}{(x_C)_w}. \qquad [80]$$

$(x_C)_{an}/(x_C)_w$ is given by [18], and [80] yields $(h'_c)_w/(h'_c)_{an} = 0.182$. For complete similarity (equal h'_c) the water rupture thickness would therefore have to be 1/0.182 times greater: 71×10^{-10} m. The corresponding change in the water rupture time is given by [75]:

$$\Delta t = -2B^{-1/2}(\sqrt{(7.1 \times 10^{-9})} - \sqrt{(1.3 \times 10^{-9})})$$

$$= -4.5 \times 10^{-5} \text{ sec.}$$

That is, the water sheet ruptures 4.5×10^{-5} sec later than it would if truly similar to the aniline sheet. In terms of a distance delay, Δx, this is 0.9 mm.

Breakup distances for such sprays are typically a few cm (Clark & Dombrowski 1972) so that this delay lies on the border of significance. Since, further, final thinning is probably faster than in the present model because of the influence of the gas stagnation point, the real delay is probably truly negligible. At higher values of U the breakup distance is less but so is Δx.

10. CONCLUSIONS

(1) Contrary to the impression given by the various empirical correlations in existence, simple criteria for the dynamic similarity of isothermal gas–liquid flows without mass transfer can be derived from the conventional governing equations. Aside from geometrical similarity of imposed velocity or pressure boundary conditions, these consist of equality of six dimensionless groups: a characteristic gas to liquid density ratio, the gas to liquid dynamic viscosity ratio and the Euler, Weber, Froude and liquid Reynolds numbers.

(2) Under certain conditions these criteria can be satisfied experimentally so that tests of their validity are possible as well as limited practical scaling, given such validity. These conditions allow a free choice of the liquid scalant as long as the vapour pressure is not high and the property group $\rho_L\sigma^3/\mu_L^4 g$ is the same for the two liquids. Once the liquid has been chosen the required length, velocity and pressure scaling is fixed as well as the molecular weight and viscosity of the gas scalant.

(3) The conventional physical model breaks down in the case of rupturing films or filaments of either phase owing to the emergence of additional van der Waals attraction effects to those of a simple surface tension, to the cooling of stretching liquid films or filaments, and to the ultimate breakdown of the continuum model. Since no general estimate of the magnitude of these effects is available the simple criteria must at present be regarded as suspect except for separated gas–liquid flow.

(4) Assuming a parallel-film model of thinning, the coalescence time of bubbles of a few mm diameter in low-viscosity liquids appears to be inertia-controlled and to be influenced to a negligible extent ($\sim 10^{-4}$ sec) by the strength of the van der Waals forces present. Actual final thinning rates will be higher than those estimated by the parallel-film model, rendering the van der Waals influences still smaller.

Whether these influences become significant for large bubbles depends critically on the final thinning rates of the non-parallel (dimpled) films involved.

(5) Given the growth of sinuous waves on a liquid sheet injected into still gas, the thinning of the sheet takes place locally as a result of both pressure variation within the sheet and shear

stress variation over it. In the final stages of thinning, shear thinning is dominant, indicating the important role of gas viscosity in sheet atomisation.

The final thinning rate is inertia controlled up to high values of the liquid viscosity ($\sim 1000\ \mu_{water}$). On a non-separated model of the gas flow the strength of the van der Waals forces appears to be of only slight influence on the rupture time/distance ($\sim 10^{-5}$ sec/1 mm). This influence should be still smaller in actual, separated flows because of an acceleration of shear thinning by the re-attachment stagnation point.

(6) In summary, the preliminary evidence on the applicability of simple similarity criteria to gas–liquid flows is favourable but considerable experimental and theoretical work is necessary before the criteria's exact range of validity can be established. In the meantime, they remain a much more fruitful basis for scaling or correlating gas–liquid phenomena than existing methods. In many situations only a few of the six similarity parameters will be of importance and the task of scaling or correlation is then less formidable.

REFERENCES

BRODKEY, R. S. 1967 *The Phenomena of Fluid Motions*, 17–2B. Addison–Wesley.

CLARK, C. J. & DOMBROWSKI, N. 1972 Aerodynamic instability and disintegration of inviscid liquid sheets. *Proc. R. Soc.* **A329**, 476–478.

CRAPPER, G. D., DOMBROWSKI, N., IEPSON, W. P. & PYOT, G. A. D. 1973 A note on the growth of Kelvin–Helmholtz waves on thin liquid sheets. *J. Fluid Mech.* **57**, 671–672.

DOMBROWSKI, N. 1962 The aerodynamic instability and disintegration of viscous liquid sheets. *Chem. Engng Sci.* **18**, 203–214.

HAGGERTY, W. W. & SHEA, J. F. 1953 A study of the stability of plane fluid sheets. *J. Appl. Mech.* **22**, 509–519.

HAMAKER, H. C. 1937 The London–van der Waals attraction between spherical particles. *Physica* **IV**, 1058–1072.

LEE, J. C. 1973 Private communication. Dept. Chem. Eng., Univ. College Swansea, Wales.

MACKAY, G. D. M. & MASON, S. G. 1963 The gravity approach and coalescence of fluid drops at liquid interfaces. *Can. J. Chem. Eng.* **41**, 203–212.

SCHELUDKO, A. 1962 Sur certaines particularités des lames mousseuses. *Kon. Akademie van Wetenschappen* **65**, 76–96.

SQUIRE, H. B. 1953 Investigation of the instability of a moving liquid film. *Br. J. Appl. Phys.* **4**, 167–169.

URSELL, F. 1956 Wave generation by wind, *Surveys in Mechanics*, pp. 217–249. Cambridge Press.

VERWEY, E. J. W. & OVERBEEK, J. T. G. 1948 *Theory of the Stability of Lyophobic Colloids*, Elsevier.

VRIJ, A. 1966 Possible mechanism for spontaneous rupture of thin free liquid films. *Disc. Farad. Soc.* **42**, 23–33.

Résumé—On montre que des critères de similitude simples, qui peuvent être expérimentalement satisfaits, peuvent être déduit des équations classiques des écoulements liquide–gaz. Ces critères sont ainsi susceptibles de vérification expérimentale et sont potentiellement utilisables pour la modélisation d'écoulements. Les équations classiques cessent cependant d'être valables si des films ou filaments se rompent, et ceci en particulier à cause de l'influence spéciale des forces de Van der Waals. Dans un cas donné, la validité des critères repose sur l'influence de tels effets spéciaux sur le développement général de l'écoulement. Deux cas sont examinés, celui de bulles coalescentes et celui de nappes liquides en cours d'atomisation, dans lesquels on montre que l'influence des forces de Van der Waals sur le temps de rupture est faible.

Auszug—Es wird gezeigt, dass einfache, experimentell ueberpruefbare Aehnlichkeitskriterien aus den herkoemmlichen Gleichungen fuer Gas-Fluessigkeitsstroemungen abgeleitet werden koennen. Die kriterien koennen deshalb durch Versuche bestaetigt und zur Modellierung von Stroemungen eingesetzt werden. Die herkoemmlichen Gleichungen verlieren jedoch ihre Gueltigkeit in Bezug auf eine Zerstoerung von Schichten oder Faeden, vor allem wegen des besonderen Einflusses von van der Waals–Kraeften. Die Gueltigkeit der Kriterien haengt in jedem einzelnen Fall vom Einfluss solcher Sondereffekte auf die allgemeine Stroemungsentwicklung ab. Zwei Faelle: das Zusammenfliessen von Blasen, und das Zerstaeuben von

Fluessigkeitsschichten, werden untersucht und es zeigt sich, dass der Einfluss der van der Waals-Kraefte auf die Zeit bis zur Zerstoerung gering ist.

Резюме—Показано, что простые критерии подобия, которые удовлетворяют эксперименту, могут быть выведены из обычных уравнений, определяющих газожидкостное течение. Эти критерии, таким образом, поддаются опытному подтверждению и потенциально полезны для измерения потоков. Показано, тем не менее, что уравнения конвекции нарушаются в условиях обрыва пленок или волокнистых струек, в частности происходящего от особого влияния ван-дер-ваальсовых сил. Ценность критериев в любом случае остается во влиянии таких особых явлений на общее развитие потока. Исследованы два случая смешения пузырей и раздробления слоев жидкости и показано, что влияние ван-дер-ваальсовых сил на время разрыва пренебрежимо.